

Tetraethylammonium Perfluorobutanesulfonate as an Alternative Salt for Electric Double Layer Capacitors

Mariana Gaško,^[a, b] Indrajit Mahadev Patil,^[a, b] Lukas Köps,^[a, b] Daniel Krüger,^[a, b] Christof Neumann,^[b, c] Andrey Turchanin,^[b, c] Fabian Alexander Kreth,^{*[a, b]} and Andrea Balducci^{*[a, b]}

The utilization of tetraethylammonium perfluorobutane sulfonate as a promising alternative salt for electrolyte solutions in electrochemical double layer capacitors is introduced in this study. A thorough analysis of the physical and electrochemical characteristics of tetraethylammonium perfluorobutane sulfonate was conducted, including the assessment of its ionic conductivity, viscosity, and thermal behavior, using a 1 M solution in acetonitrile. Comparative assessments were made between the performance of this novel electrolyte and two well-studied electrolytes: 1 M tetraethylammonium tetrafluoro-

borate and 1 M tetraethylammonium bis(trifluoromethanesulfonyl)imide in acetonitrile, focusing on electrochemical performance and long-term stability. Furthermore, an investigation into the impact of tetraethylammonium perfluorobutane sulfonate on the anodic dissolution of aluminum current collectors was conducted. The results highlight the potential of tetraethylammonium perfluorobutane sulfonate as an effective replacement for bis(trifluoromethanesulfonyl)imide-based electrolytes.

Introduction

Electrochemical double layer capacitors (EDLCs), also known as supercapacitors or ultracapacitors, have attracted considerable interest in recent years due to their outstanding power density and cycling stability.^[1] The storage mechanism of EDLCs is based on non-Faradic processes consisting of the electrostatic separation of charges at the electrode-electrolyte interface, forming an electrical double layer.^[2] As a result, EDLCs benefit from very short charge and discharge times (within seconds), high power outputs (up to 10 kW kg^{-1}), and excellent cycle life ($> 1,000,000$ cycles).^[1a,3] The most recent systems use carbide-derived carbon as the active materials and non-aqueous electrolytes that contain quaternary ammonium salts, such as tetraethylammonium tetrafluoroborate (TEABF_4), in acetonitrile

(ACN) or propylene carbonate (PC).^[4] These electrolytes enable an operative voltage of 2.85–3.0 V.^[3] However, despite these advantages, EDLCs still need to increase their overall energy density which is in the range of $\approx 10 \text{ Wh kg}^{-1}$.^[3,5] To reach this goal, the realization of devices with higher operating voltage compared to the state-of-the-art appears as the most straightforward strategy.^[1c] The electrolyte degradation observed at voltages above 3 V adversely affects the performance of the state-of-the-art electrolyte (1 M TEABF_4 in ACN), resulting in significant capacitance fading and consequent degradation of the cycle life performance. This subsequently precludes the enhancement of the overall energy density. Therefore, the primary limitation on both operative voltages, and consequently, the energy density of the cell, is directly related to the electrochemical stability of the electrolyte.^[6]

In recent years, studies have shown that the development of new electrolytes consisting of alternative conducting salts in conventional solvents could be the key to achieving high-voltage EDLCs.^[7] Replacing the anion BF_4^- with bis(trifluoromethanesulfonyl) imide (TFSI⁻) results in several favorable properties.^[7a,8] The use of tetraethylammonium bis(trifluoromethanesulfonyl) imide (TEATFSI) in ACN has been proven to enhance the electrochemical stability range and offer improved long-term cycling performance at voltages above 3 V.^[7c] However, TFSI-based electrolytes still encounter difficulties in passivating aluminum (Al) current collectors, leading to anodic dissolution at operating voltages higher than 3 V and, consequently, a reduction in the overall energy density.^[9] In fact, it is known that the pitting corrosion of Al current collectors depends on the solubility of the formed complex aluminum bis(trifluoromethanesulfonyl) imide $[\text{Al}(\text{TFSI})_3]$ in the electrolyte.^[10] Several TFSI-based ionic liquids (ILs), such as N-butyl-N-methylpyrrolidinium bis(trifluoromethanesulfonyl) imide (PYR₁₄TFSI), can passivate the Al surface, preventing anodic dissolution. In

[a] M. Gaško, I. Mahadev Patil, L. Köps, D. Krüger, F. A. Kreth, Prof. A. Balducci
Institute for Technical Chemistry and Environmental Chemistry, Friedrich Schiller University
Jena, Philosophenweg 7a, 07743 Jena, Germany
E-mail: fabian.alexander.kreth@uni-jena.de
andrea.balducci@uni-jena.de

[b] M. Gaško, I. Mahadev Patil, L. Köps, D. Krüger, C. Neumann, A. Turchanin, F. A. Kreth, Prof. A. Balducci
Center for Energy and Environmental Chemistry Jena (CEEC Jena), Friedrich Schiller University Jena, Philosophenweg 7a, 07743 Jena, Germany

[c] C. Neumann, A. Turchanin
Institute of Physical Chemistry, Friedrich Schiller University Jena, Lessingstraße 10, 07743 Jena, Germany

Supporting information for this article is available on the WWW under <https://doi.org/10.1002/batt.202400283>

© 2024 The Authors. *Batteries & Supercaps* published by Wiley-VCH GmbH. This is an open access article under the terms of the Creative Commons Attribution Non-Commercial License, which permits use, distribution and reproduction in any medium, provided the original work is properly cited and is not used for commercial purposes.

contrast, the increased solubility of $[\text{Al}(\text{TFSI})_3]$ in polar solvents has been shown to inhibit the formation of a protective layer, leading to corrosion onset.^[10c,11] Recent studies also indicate that the prior addition of $[\text{Al}(\text{TFSI})_3]$ to an electrolyte can reduce or eliminate the anodic dissolution of Al current collectors, thereby increasing electrode stability.^[7a,b]

Given the aforementioned considerations, the development of novel electrolytes is of paramount importance. The proposed electrolyte should combine the favourable attributes of both TEABF₄ and TEATFSI, which are known for their exceptional transport properties and widened electrochemical stability window, respectively. Also, it is imperative that this new electrolyte effectively addresses the adverse effects, such as voltage operation limitations, which have been a significant challenge in the past, to enable an elevation in energy density. Furthermore, mitigating concerns such as the persistent dissolution of Al current collectors, which undermines long-term cell performance, is imperative. These advancements are indispensable for augmenting the overall efficiency of EDLCs. Previous studies have demonstrated that the perfluorobutane-sulfonate anion (PFBS⁻) can be successfully incorporated into ILs [1,3,7] or ionic liquid gel polymer electrolytes. Good electrochemical and thermal stability, as well as good ionic conductivity, can be achieved by using these electrolytes.^[12] To the best of our knowledge, however, no research has been conducted on PFBS⁻-based electrolytes for application in EDLCs. This work introduces tetraethylammonium perfluorobutanesulfonate (TEAPFBS) as an alternative salt for EDLCs. Investigating the physical and electrochemical properties of TEAPFBS, ionic conductivity, viscosity, and thermal behaviour of a 1 M solution containing TEAPFBS in ACN are considered in detail. Furthermore, the performance of this electrolyte in EDLCs has been assessed by analyzing its electrochemical performance and cycling stability and compared to that of 1 M TEABF₄ and 1 M TEATFSI in ACN. Finally, the impact of TEAPFBS on the anodic dissolution of Al current collectors was studied to determine its suitability as a replacement for existing electrolytes for EDLCs.

Result and Discussion

Figure 1 is comparing the transport properties, including ionic conductivity and viscosity, as well as the thermal behavior, of the investigated ACN-based electrolytes. The ionic conductivity was measured from -30 to 80°C (Figure 1a). Among the electrolytes tested, the conventional electrolyte TEABF₄ in ACN showed the highest conductivity across the temperature range, whereas TEAPFBS exhibited the lowest conductivity. At -30°C , the conductivities of the electrolytes containing TEABF₄, TEATFSI, and TEAPFBS were 25 , 19 , and 16 mS cm^{-1} , respectively. As the temperature increases, the conductivity increases accordingly, as expected. The elevated temperatures result in an increase in ion mobility, accompanied by a reduction in the viscosity of the solvent. These developments facilitate better ion transport through the electrolyte, as the resistance to this process is reduced. At 20°C , the electrolyte 1 M TEABF₄ in ACN shows a conductivity of 47 mS cm^{-1} . Meanwhile, the electrolytes

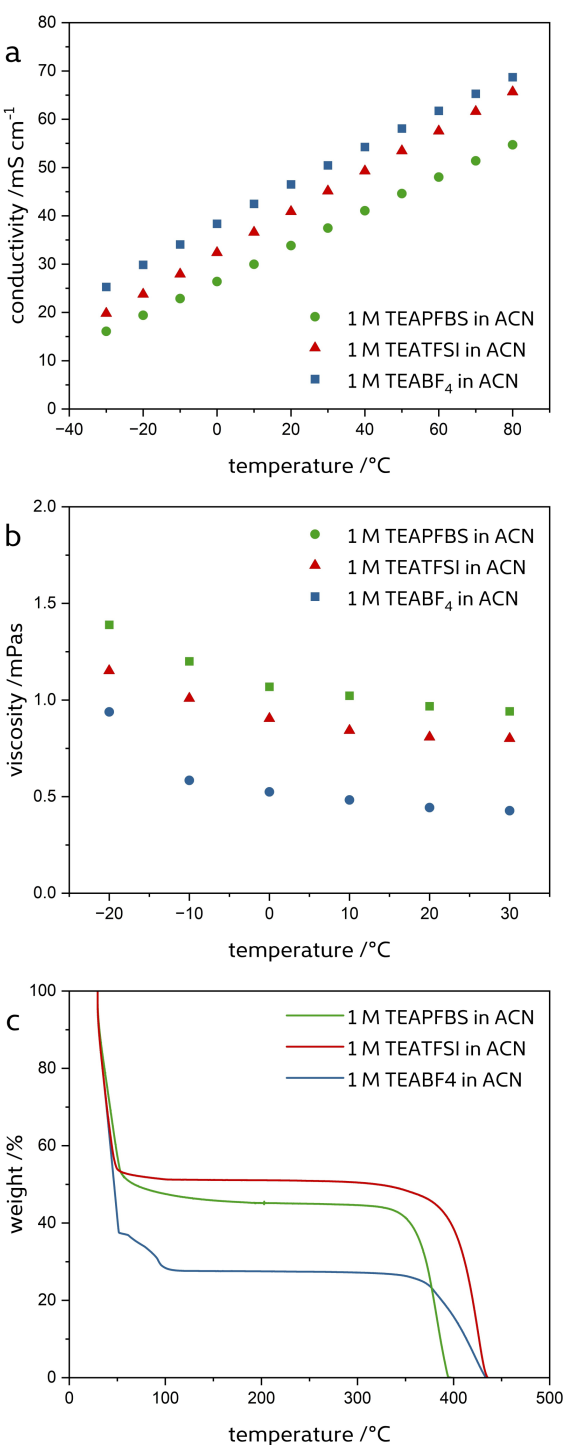


Figure 1. Representation of the (a) ionic conductivity within the temperature range of -30°C to 80°C , the (b) viscosity within the temperature range of -20°C to 30°C and the (c) thermal behavior within the temperature range of 0°C to 500°C of 1 M TEABF₄ in ACN, 1 M TEATFSI in ACN and 1 M TEAPFBS in ACN.

containing TEATFSI and TEAPFBS display conductivities of 41 and 38 mS cm^{-1} , respectively. Based on the viscosity properties shown in Figure 1b, it can be observed that the electrolytes investigated herein show a similar trend. In the temperature range of -20 to 30°C , the viscosity increases in the following

order: $\text{TEABF}_4 < \text{TEATFSI} < \text{TEAPFBS}$. The electrolytes containing TEABF_4 , TEATFSI , and TEAPFBS show viscosity values ranging from 0.95, 1.20, and 1.4 mPa s at -20°C to 0.45, 0.85, and 1.00 mPa s at 20°C . As temperature increases, the viscosity decreases, which is expected. Both measurements confirm the improvement in transport properties with increasing temperature. Given that the same salt concentration is used across all examined systems, these properties are primarily influenced by the solvent in use. In this context, the use of ACN in all three systems helps to elucidate the comparable results observed among the electrolytes. Hence, in terms of conductivity and viscosity, the utilization of 1 M TEAPFBS in ACN is comparable to the state-of-the-art electrolyte and thus appears suitable for EDLCs.

The TGA measurements (Figure 1c) show a significant decrease in mass between $30\text{--}50^\circ\text{C}$ for all three ACN-based electrolytes, which is attributed to the evaporation of volatile ACN. Unlike TFSI^- - and PFBS^- -based electrolytes, where ACN evaporation is complete at around 50°C , the conventional electrolyte experiences a reduction in evaporation rate from 50 to 100°C . Previous studies have documented similar behavior of TEABF_4 in ACN.^[6c] After complete evaporation of ACN, a linear region up to ca. 350°C is observed for the investigated electrolytes. This region is attributed to the thermal stability of the conducting salt, which is the only remaining component. At 440°C all components are decomposed. Since commercial EDLCs are not operated above 70°C , differences in thermal stability between $320\text{--}350^\circ\text{C}$ can be neglected.^[3,13] The conventional electrolyte experiences a higher mass loss due to its larger ACN mass fraction rather than the thermal stability of the conductive salt TEABF_4 . Overall, 1 M TEAPFBS in ACN was shown to have comparable thermal behavior to 1 M TEABF_4 and 1 M TEATFSI in ACN.

Optimizing the long-term functionality of EDLCs requires a comprehensive investigation of the electrochemical properties of their electrolyte (see Figure 2). Therefore, the positive and negative potential limits of the ACN-based electrolytes were determined and are shown in Figure 2a. As the same cation is used in all three electrolytes, the negative potential limit of $-1.75\text{ V vs. Ag}^+/\text{Ag}$ is the same for all systems. In contrast, the positive potential limit varies depending on the anion, following the order of: $\text{PFBS}^- < \text{TFSI}^- < \text{BF}_4^-$. The electrolytes containing TEAPFBS , TEATFSI , and TEABF_4 display positive potential limits of 0.9, 1.1, and 1.15 V vs. Ag^+/Ag , respectively. Consequently, the electrolyte exhibiting the widest operating voltage (OPV) window is the state-of-the-art electrolyte. Nevertheless, given the small differences in the negative potential limits, 1 M TEAPFBS in ACN can be considered to have a comparable electrochemical voltage range to 1 M TEATFSI and 1 M TEABF_4 in ACN. To facilitate a comprehensive comparison of the investigated electrolytes in terms of their electrochemical performance, the specific energy and specific power of symmetrical EDLCs for all three cells have been presented in a Ragone plot (Figure 2b). By applying upper voltage limits of 2.7 V and 3.0 V, it is evident that the examined electrolytes demonstrate comparable performance, indicating similar energy and power values under the same operational conditions.

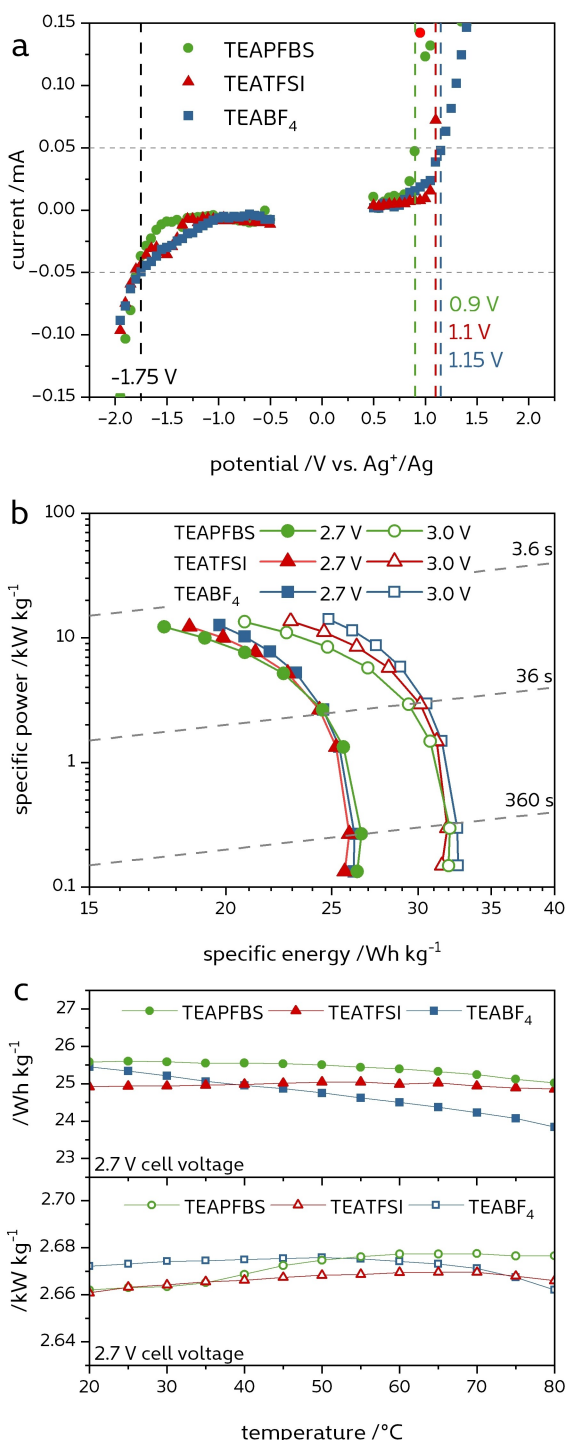


Figure 2. Comparison of electrochemical performance: a) Representation of the measured current during floating as a function of the potential limit reached for 1 M TEABF_4 in ACN, 1 M TEATFSI in ACN, and 1 M TEAPFBS in ACN. The dashed lines mark the maximum potential limits determined; b) Ragone-diagram comparing specific energy and specific power; and c) temperature-dynamic evolution of energy and power for a cell voltage of 2.7 V.

This observation is further substantiated by an examination of the temperature dependence of specific energy and specific power (Figure 2c), which reveals consistent performance trends across all three electrolytes. When polarized to 2.7 V, it is

evident that a slight decrease in energy is observed with increasing temperature, while the power increases slightly. Similar trends are observed for 3 V polarization (see Figure S4). While the observed increase in power can be attributed to the improved transport properties of the electrolyte at higher temperatures, the decrease in energy is likely caused by the limited thermal stability of the ACN solvent. These trends correspond well with a previous work from our group.^[14] Additional cyclic voltammograms and voltage profiles of symmetric EDLCs containing the electrolytes considered in this study demonstrate a consistent non-faradic behavior and are shown in Figure S5 and S6 of the Supporting Information. These results clearly indicate that the herein presented salt, TEAPFBS, exhibits similar electrochemical performance to TEATFSI and TEABF₄.

To further investigate the effect of the considered electrolytes on EDLC stability, floating tests on devices containing the three electrolytes were conducted at 2.7 V (Figure 3a) and 3.0 V (Figure 3b). The latter was chosen due to previous indications that the state-of-the-art electrolyte TEABF₄, and its most promising alternative, TEATFSI, exhibit poor cell performance at voltages exceeding 3 V. Hence, evaluating the performance of TEAPFBS under these conditions appears imperative. After floating at 2.7 V for 500 h, all three tested EDLCs were able to maintain 96% of their initial capacitance, as shown in Figure 3a. This result is to be expected, as the electrolytes are electro-

chemically stable at this voltage and no decomposition processes occur. A comparison of the impedance spectra of the electrolytes containing TEAPFBS, TEATFSI, and TEABF₄ (Figure 3c–e) before and after floating at 2.7 V shows no pronounced differences, confirming the stability of the systems considered.

Increasing the floating voltage to 3.0 V results in different long-term cell behavior. Figure 3b indicates a strong dependency of the electrolyte and electrode stability on the delivered capacitance. The cell containing the state-of-the-art electrolyte exhibits the highest capacitance retention of 90 %, whereas 1 M TEATFSI in ACN only retains 67% of its initial capacitance. The observed difference can be explained by the evolution of the impedance spectra after floating at 3.0 V. For TEABF₄, the impedance remains stable (Figure 3e), indicating that there is no change in the electrolyte's composition. However, the drastic drop in capacitance observed in TEATFSI is related to a noticeable increase in grain boundary resistance (Figure 3d). This increase in impedance is likely due to the dissolution of the Al current collectors and the formation of TFSI⁻ decomposition products.^[9b] In comparison to the TEATFSI-based cell, the cell containing 1 M TEAPFBS in ACN experiences less pronounced capacitance fading. The latter gradually loses capacitance throughout the floating experiment, retaining 77% of its initial capacitance at the end. The impedance spectra of TEAPFBS (Figure 3c) show a less prominent evolution of the semi-circle

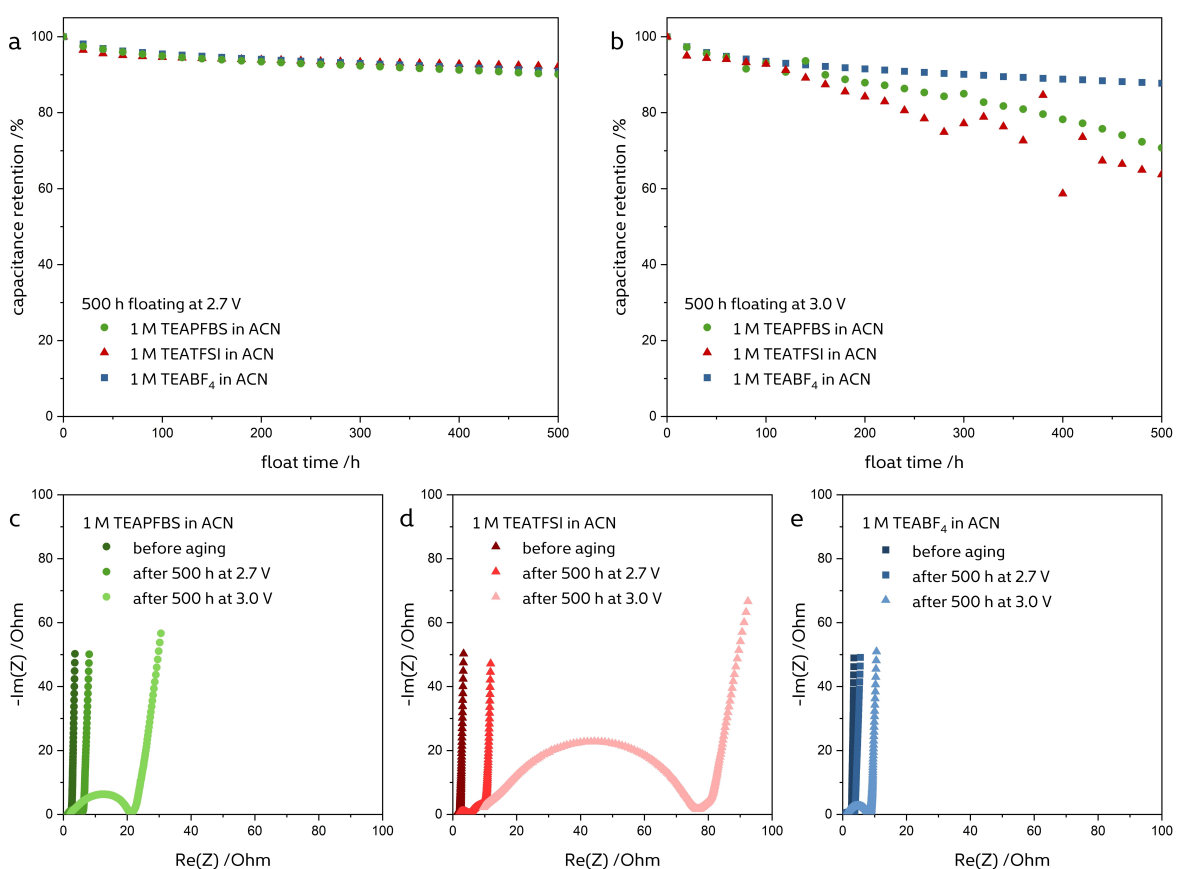


Figure 3. Comparison of the capacitance retention obtained by float tests carried out at (a) 2.7 V and (b) 3.0 V. Evolution of the impedance spectra of the EDLCs that contain (c) 1 M TEABF₄ in ACN, (d) 1 M TEATFSI in ACN and (e) 1 M TEAPFBS in ACN.

compared to TEATFSI, indicating higher electrochemical stability. In the case of TEAPFBS, the slight increase in grain boundary resistance may be attributed to either the formation of electrolyte decomposition products or the beginning of anodic dissolution.

The process of anodic dissolution was further examined by applying a constant potential of 1.7 V vs. Ag^+/Ag to pristine aluminum discs and monitoring the resulting cumulative current evolution. As shown in Figure 4a, the choice of conductive salt has a decisive influence on the electrochemical behavior and stability of the respective electrolytes. The state-of-the-art electrolyte displays the most desirable properties. A consistent cumulative current of near 0 mAh is observed, confirming the absence of pitting corrosion in Al current collectors, and highlighting its robust electrochemical stability, as previously discussed. In the case of TEAPFBS, a steady rise in the obtained current is noted until it reaches a peak value of 4.2 mAh. The increase in current indicates the occurrence of faradic reactions due to oxidation of the aluminum current collector. However, given the modest increase in current and impedance (Figure 3c), it is suggested that the formation of decomposition products may play a role in partially passivating the Al current collectors. This may also clarify why the cells containing TEAPFBS exhibit superior performance compared to the TEATFSI-based cells. The electrolyte 1 M TEATFSI in ACN exhibited the most significant rise in cumulative anodic dissolution current, achieving 10 mAh within the initial 4 h. In the end, a current of 12 mAh was obtained, which is three times greater than the current obtained with the cell containing TEAPFBS. In good agreement, SEM images (Figure 4b-d) show that pitting corrosion increases in the order of $\text{BF}_4^- < \text{PFBS}^- < \text{TFSI}^-$. While the BF_4^- based cell exhibits no visual indication of anodic dissolution, PFBS⁻ displays locally restricted, round perforations. In contrast, the TFSI⁻ based cell demonstrates both frayed perforations and extensive pitting corrosion of the Al surface. Hence, the poor performance of 1 M TEATFSI in ACN can be attributed to the ongoing anodic dissolution process of the Al current collectors. Based on the results obtained, it can be concluded that 1 M TEAPFBS in ACN is less susceptible to the pitting corrosion of Al current collectors and therefore provides superior long-term performance compared to 1 M TEATFSI in ACN.

To gain detailed insight into the characteristics of the aluminum passivation and dissolution reactions, X-ray photo-electron spectroscopy (XPS) measurements were performed on the previously shown Al current collectors. The respective high resolution F 1s, O 1s, Al 2p spectra are shown in Figure 5a-c. Complementary XPS information can be found in Tables S1 to S3 of the Supporting information.

Aluminum is typically considered corrosion-resistant due to the formation of an oxide layer on its surface upon exposure to air. In addition to this oxide layer, the aluminum current collector's dissolution resistance can be enhanced by a passivation layer composed of aluminum fluoride. This layer of aluminum fluoride requires the fluorination of the current collectors through the decomposition of electrolyte compounds. Recent studies have highlighted the significant impact

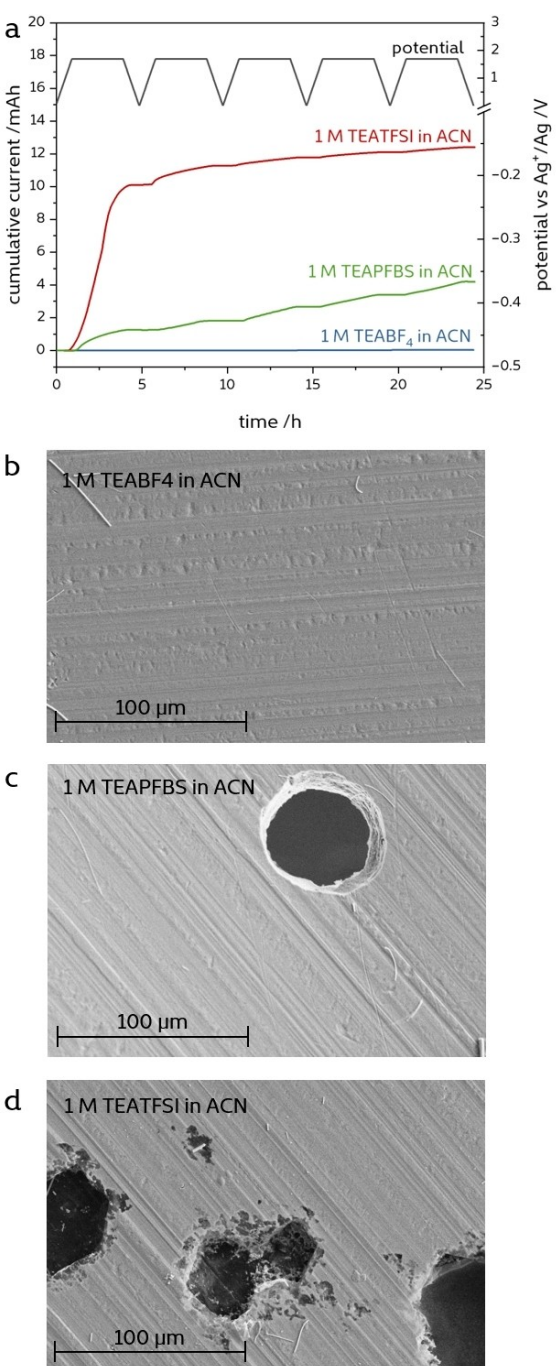


Figure 4. Anodic dissolution of Al current collector. a) Evolution of the cumulative current during the application of a constant voltage of 1.7 V vs. Ag^+/Ag for 1 M TEABF₄ in ACN (blue), 1 M TEATFSI in ACN (red), and 1 M TEAPFBS in ACN (green). b-d) Respective SEM images obtained after anodic dissolution tests (all 500x magnification).

of the electrolyte on the aging behavior of aluminum current collectors, emphasizing that both the solvent and the salt ions play crucial roles in the degradation processes. The solubility of aluminum complexes, the primary cause of anodic dissolution, is influenced by the dielectric constant of the solvent and the concentration of dissolved compounds, thereby affecting the degree of anodic dissolution. Furthermore, the extent of anodic

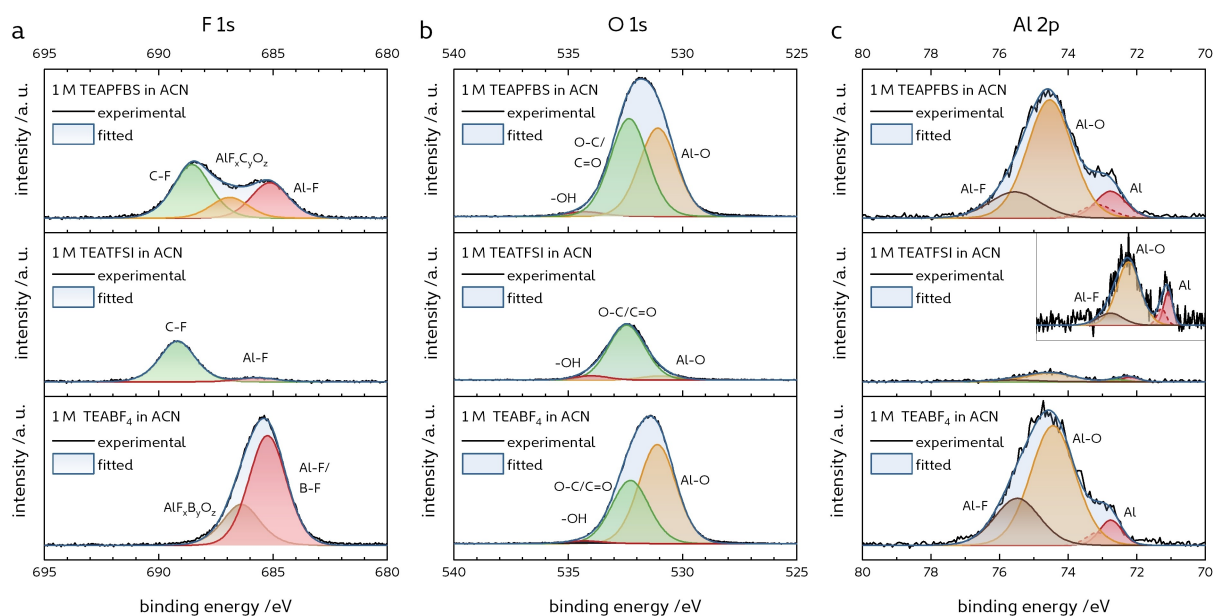


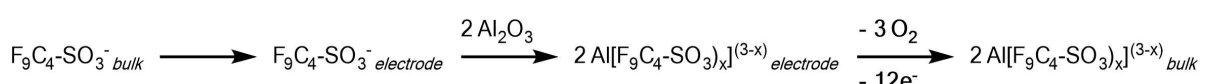
Figure 5. High resolution XP spectra of Al current collectors subjected to extensive anodic dissolution in 1 M TEAPFBS (top) in ACN, 1 M TEATFSI in ACN (middle), and 1 M TEABF₄ in ACN (bottom): a) F 1s spectra, b) O 1s spectra, and c) Al 2p spectra.

dissolution is strongly dependent on the type of anion present, as different anions have differing abilities to form soluble aluminum complexes.^[6a] In the past, the interaction of TFSI⁻ and BF₄⁻ based electrolytes with aluminum current collectors has been extensively examined. Whereas BF₄⁻ is known to create a stable AlF₃ passivation layer, TFSI⁻ forms a soluble [Al(TFSI)₃] complex.^[10] The latter has been proposed as a multi-step reaction at the aluminum surface, starting with the adsorption of TFSI⁻ anions, reaction with the Al₂O₃ passive film, followed by the formation of the [Al(TFSI)₃] complex, and its subsequent diffusion away from the surface.^[15] These processes are in good agreement with the obtained XP spectra (corresponding binding energies are summarized in Table S1 to S3). For electrolytes based on TEABF₄, the XP spectra display signals for Al–F (685.3 eV) and Al–O (531.1 eV) bonds, suggesting the formation of a passivation layer. In contrast, the spectra for TEATFSI-based electrolytes predominantly reveal the presence of C–F (689.2 eV) bonds, indicative of residual adsorbed TFSI⁻ anions on the electrode surface. Interestingly, the behavior of the TEAPFBS-based electrolyte exhibits characteristics which can be assigned to both passivation and dissolution mechanisms. XPS analysis reveals both C–F and Al–F signals, suggesting that both passivation and dissolution processes of the aluminum current collector occur simultaneously. Additionally, the F 1s spectrum shows a distinct signal at 686.9 eV, attributed to a compound composed of AlF_xC_yO_z. This signal likely represents an intermediate product arising from the adsorption of the

PFBS⁻ anion and the potential formation of an [Al(PFBS)_x]^(3-x) complex. Following the Al dissolution reaction mechanism for TFSI⁻ based electrolytes initially proposed by X. Wang et al.,^[15] a similar mechanism can be suggested for PFBS⁻ based electrolytes (Scheme 1).

Conclusions

This work underlines the crucial role of identifying alternative conductive salts in the advancement of EDLCs, thereby expanding their potential application. An essential requirement for this progress is the development of an electrolyte with both, superior transport properties and high electrochemical stability. This study effectively demonstrates the successful use of TEAPFBS in combination with ACN as an alternative electrolyte, with comparable conductivity and viscosity to the state-of-the-art electrolyte TEABF₄ in ACN. The use of 1 M TEAPFBS in ACN allows the realization of EDLCs with excellent cycling stability at a voltage of 2.7 V. Furthermore, EDLCs containing this electrolyte sustain 77% of their initial capacitance after floating for 500 h at 3.0 V. Notably, our results indicate that the incorporation of TEAPFBS does not outperform the conventional TEABF₄ electrolyte. It does, however, outperform one of the most promising alternative electrolytes comprising TEATFSI in ACN, particularly in terms of long-term stability at 3 V. It has been shown that this electrolyte does not cause anodic



Scheme 1. Proposed reaction scheme of Al dissolution by the PFBS⁻ anion.

dissolution of the Al current collectors to the same extent as TEATFSI, indicating higher electrochemical stability. Given the increased efforts to replace the conventional salt LiPF₆ in lithium ion batteries due to its inadequate safety performance, coupled with the widely documented oxidation of Al current collectors attributed to LiTFSI, the search for a viable alternative is becoming paramount. The results presented in this study suggest that the incorporation of PFBS⁻ anions into Li-containing electrolytes could serve this purpose. Therefore, a comprehensive investigation of the anion PFBS and its potential integration into Li-based electrolytes for LiBs appears of interest and should be considered in the future.

Experimental Section

Synthesis of Tetraethylammonium Perfluorobutanesulfonate

Tetraethylammonium perfluorobutanesulfonate (TEAPFBS) was prepared by the metathesis reaction of potassium perfluorobutanesulfonate (KPFBS) and tetraethylammonium bromide (TEABr) (Scheme 2).

KPFBS (5.0 g, 0.015 mol) and TEABr (3.1 g, 0.015 mol) were suspended in a solution of dichloromethane (DCM, 25 mL) and ethanol (25 mL). The reaction mixture was stirred at room temperature for 48 h. The organic layer was collected, and the aqueous layer was extracted twice with DCM (25 mL). The combined organic layers were washed several times with 50 mL H₂O until the addition of AgNO₃ to the aqueous phase no longer resulted in the precipitation of AgBr. The solvent was removed under reduced pressure using a rotary evaporator (500 mbar, 40 °C). The product was dried under vacuum (10⁻¹ mbar) for 20 h. TEAPFBS was obtained as a white solid (4.8 g, 0.010 mol, 67%). ¹H-NMR (400 MHz, CD₃CN): δ = 1.20 (tt, 12 H, CH₃, J(7.27, 1.20)), 2.16 (s, H₂O), 3.16 (q, 8 H, -CH₂-, J(7.27)) ppm. ¹³C-NMR (100.6 MHz, CD₃CN): δ = 7.6 (CH₃), 53.0 (N-CH₂-) ppm. ¹⁹F-NMR (376.5 MHz, CD₃CN): δ = -126.6 (s, 2 F, CF₂), -122.2 (s, 2 F, CF₂), -115.7 (s, 2 F, CF₂), -81.8 (s, 3 F, CF₃) ppm. Corresponding NMR spectra are shown in Figure S1–S3 of the Supporting Information. ICP-OES analysis of the salt confirmed the high purity of the synthesized TEAPFBS by the absence of a K signal at 766.49 nm.

Electrolyte Preparation

To ensure a water content below 20 ppm, the solvent acetonitrile (ACN, CAS: 75-05-08, purity ≥99.8%, Sigma-Aldrich) was dried over molecular sieves (3 Å) and verified through Karl-Fischer titration. The conducting salts tetraethylammonium tetrafluoroborate (TEABF₄) and tetraethylammonium bis(trifluoromethanesulfonato)imide (TEATFSI) were purchased from Sigma Aldrich and used as received. Tetraethylammonium perfluorobutanesulfonate was syn-

thesized as previously described. The salts were dried in a B-585 glass vacuum oven (BÜCHI) for 24 h at 120 °C and 10⁻² mbar. Electrolytes consisting of a 1 M solution of the conducting salts in ACN have been prepared and stored inside an argon-filled glovebox.

Physicochemical Characterization

The ionic conductivities of each electrolyte were measured using a Binder KB53 climatic chamber and a BioLogic MPG-2 potentiostat as indicated elsewhere.^[16] The dependence of temperature on conductivity was investigated over a temperature range from -30 °C to 80 °C. The viscosity values were determined using an Anton-Paar MCR 102 rotational viscometer within the temperature range of -20 °C to 30 °C as described in a previous work.^[16] The shear rate was set to 1000 s⁻¹. Thermogravimetric analysis (TGA) was used to assess the thermal stability of the electrolytes using a PerkinElmer TGA 4000 according to the procedure reported before.^[17] The temperature was increased by 10 °C per minute from 30 °C to 440 °C.

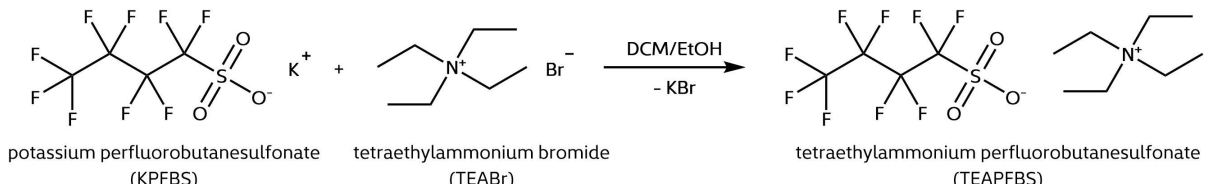
The measurements were carried out in a Swagelok-type cell using two identical activated carbon (AC) electrodes supplied by Skeleton Technologies. As both sides of the electrodes were coated with AC, one side was removed prior to measurement, resulting in electrodes with a mass loading of 7.3 mg cm⁻². The cells were assembled inside a MBRAUN LABmaster pro glove box filled with argon and less than 1 ppm of both H₂O and O₂. The electrodes were separated by Whatman GF/D glass microfiber filters (thickness of 520 µm), which were saturated with 120 µL of the respective electrolyte.

Spectroscopic Characterization

1D (¹H, ¹³C, and ¹⁹F) nuclear magnetic resonance (NMR) spectra were recorded on a Bruker Avance III. Whereas the chemical shifts for ¹H and ¹³C are reported as ppm downfield from SiMe₄, for ¹⁹F they are provided in ppm upfield from PhCF₃. ICP-OES measurements were performed on an Agilent 5800 ICP-OES scanning for the K signal at 766.49 nm. SEM images were taken with a Zeiss Sigma VP at a beam energy of 10 kV using the Everhart-Thornley detector of the system. XPS was performed using a K-Alpha X-ray Photoelectron Spectrometer System (Thermo Fisher Scientific) with a monochromatic X-ray source (Al K_α) with a spot diameter of 400 µm and an electron detector with 0.5 eV energy resolution. A flood gun was employed for charge compensation. The spectra were calibrated using the C 1s peak (284.6 eV) and fitted using Voigt functions after background subtraction.

Electrochemical Characterization

The electrochemical stability of the herein-investigated electrolytes was evaluated by identifying their positive and negative potential limits. Therefore, the respective operating voltage has been determined by cyclic voltammetry (CV) and float test utilizing a



Scheme 2. Synthesis of tetraethylammonium perfluorobutanesulfonate (TEAPFBS) from potassium perfluorobutanesulfonate (KPFBS) and tetraethylammonium bromide (TEABr).

Biologic VMP3. For this, three-electrode Swagelok-type cells have been used, comprising an AC electrode (Skeleton Technologies) as working electrode (WE), an oversized AC electrode as counter-electrode (CE, active mass higher than 40 mg), and a silver (Ag) wire as the quasi-reference electrode (RE). Rate tests for the Ragone plot were performed by galvanostatic charge-discharge measurements at current densities ranging from 0.05 A g^{-1} to 5 A g^{-1} . In each case, the reported capacitance or capacity values were normalized to the total mass of active material. Temperature dynamic measurements were performed in a temperature range from 20°C to 80°C according to a procedure described elsewhere.^[14,18] The determination via float test was conducted by applying a constant potential for 30 min, followed by a subsequent increase of voltage limits ranging from $\pm 0.5 \text{ V}$ vs. Ag^+/Ag to $\pm 2.0 \text{ V}$ vs. Ag^+/Ag . No significant current is detected if the potential limit is set below the system's maximum voltage. However, exceeding the devices voltage limit requires a measurable current flow to maintain the potential due to electrolyte degradation.^[19] To assess the impact of electrolyte stability on EDLC performance at different voltages, float tests were conducted using full-cells comprising two identical AC electrodes (Skeleton Technologies). The cells were charged to the potential of 2.7 V and 3.0 V and held at those potentials for a total time of 500 h. Each 20 h five galvanostatic charge-discharge cycles were performed. Electrochemical impedance spectroscopy (EIS) measurements were performed before and after 500 h of floating within a frequency range of 100 kHz to 10 mHz to monitor the evolution of the internal resistance and its impact on the specific capacitance of the cells. The measurements were carried out utilizing a Biologic VMP3 and MPG2, with the same cell setup as for the physicochemical characterization. To investigate the effect of the respective electrolytes on the anodic dissolution of aluminum (Al) current collectors, Al metal discs (12 mm diameter) were used as the working electrode, an oversized activated carbon electrode as the counter electrode and an Ag-wire as a reference electrode.^[9c] In this experiment, a custom CV measurement was used to polarise the Al disc until its peak potential of 4.2 V vs. Li^+/Li was reached. The scan rate was set to 0.5 mV s^{-1} . Before reversing the scanning direction, the maximum potential was maintained for 3 h. This cycle was repeated ten times for a total of 30 h at maximum voltage. Integration of the resulting current over the experimental period allowed the calculation of the cumulative anodic dissolution current.

To estimate the specific capacitance C the following equation has been used (Eq. 1):

$$C = \frac{I}{\frac{dV(t)}{dt} m} \quad (1)$$

in which I represents the applied current, m the active mass of the electrode and $\frac{dV(t)}{dt}$ the slope of the charge/discharge curve obtained from galvanostatic cycling with potential limitation (GPL).^[20]

The maximum power P_{max} and maximum energy E_{max} were determined from the galvanostatic charge-discharge measurements according to a procedure described elsewhere.^[21] The instantaneous power $p(t)$ was determined from the product of the instantaneous voltage $v(t)$ and current $i(t)$. While P_{max} has been estimated by the maximum of the modulus function of the discharge semi-period of $p(t)$, E_{max} has been evaluated by integration of $p(t)$ during the discharge period.

$$P_{max} = \max\{|p(t)|\} = \max\{|v(t)i(t)|\} \quad (2)$$

$$E_{max} = \int_{t_0}^{t_n} p(t) dt = \int_{t_0}^{t_n} v(t)i(t) dt \quad (3)$$

with the initial time t_0 and the final time of the discharge semi-period t_n .

Acknowledgements

First and foremost, we would like to thank Beate Fähndrich, Zhong Zheng, and Sri Rezeki for their assistance during this work. The authors would also like to acknowledge the financial support from the Friedrich-Schiller-University Jena (FSU Jena). F. K. and A. B. would like to thank the financial support from Deutsche Forschungsgemeinschaft (DFG) the project "New Electrolytes for Capacitive Electrochemical Storage" (BA4956/16-1). I. M. P and A. B. would like to thank the European Union's Horizon Europe research and innovation program (GREENCAP 101091572). The authors acknowledge Stephanie Höppener and Ulrich S. Schubert for providing access to the scanning electron microscope. The SEM facilities of the Jena Center for Soft Matter (JCSM) were established with a DFG grant. Further, the Authors would like to acknowledge the European Fonds for Regional Development (Europäischer Fonds für Regionale Entwicklung; EFRE-OP 2014–2020; Project No. 2021 FGI 0035, NanoLabXPS). Open Access funding enabled and organized by Projekt DEAL.

Conflict of Interests

The authors declare no conflict of interest.

Data Availability Statement

The data that support the findings of this study are available from the corresponding author upon reasonable request.

Keywords: acetonitrile • anodic dissolution • conducting salt • EDLC • electrolyte

- [1] a) A. A. Brandt, S. Pohlmann, A. Varzi, A. Balducci, S. Passerini, *MRS Bull.* **2013**, *38*, 554–559; b) B. T. Kim, G. Jung, S. Yoo, K. S. Suh, R. S. Ruoff, *ACS Nano* **2013**, *7*, 6899–6905; c) C. P. Simon, Y. Gogotsi, *Nat. Mater.* **2008**, *7*, 845–854.
- [2] a) A. G. Wang, L. Zhang, J. Zhang, *Chem. Soc. Rev.* **2012**, *41*, 797–828; b) F. Cheng, X. Yu, J. Wang, Z. Shi, C. Wu, *Electrochim. Acta* **2016**, *200*, 106–114; c) C. G. H. Lane, E. Jezek, *Electrochim. Acta* **2014**, *150*, 173–187; d) D. F. A. Kreth, A. Balducci, in *Reference Collection in Chemistry, Molecular Sciences and Chemical Engineering*, Elsevier Inc., **2024**, 428–443.
- [3] Skeleton Technologies, SkelCap Supercapacitor Data Sheet, <https://1188159.fs1.hubspotusercontent-na1.net/hubfs/1188159/02-DS-220909-SKELCAP-CELLS-1D.pdf>, accessed 2023.
- [4] a) A. L. Köps, P. Ruschhaupt, C. Guhrenz, P. Schlee, S. Pohlmann, A. Varzi, S. Passerini, A. Balducci, *J. Power Sources* **2023**, *571*, 233016; b) B. A. Krause, A. Balducci, *Electrochim. Commun.* **2011**, *13*, 814–817.
- [5] A. Balducci, *J. Power Sources* **2016**, *326*, 534–540.
- [6] a) A. E. Pameté, L. Köps, F. A. Kreth, S. Pohlmann, A. Varzi, T. Brousse, A. Balducci, V. Presser, *Adv. Energy Mater.* **2023**, *2301008*; b) B. F. A. Kreth, L. H. Hess, A. Balducci, *Energy Storage Mater.* **2023**, *56*, 192–204; c) C. L. Köps, F. A. Kreth, A. Bothe, A. Balducci, *Energy Storage Mater.* **2022**, *44*, 66–72; d) D. R. Kost, F. A. Kreth, A. Balducci, *ChemElectroChem* **2024**, *11*,

- e202300823; e) E. N. Ma, D. Yang, S. Riaz, L. Wang, K. Wang, *Technologies* **2023**, *11*, 38.
- [7] a) A. J. Krummacher, A. Balducci, *Chem. Mater.* **2018**, *30*, 4857–4863; b) B. J. Krummacher, L. H. Hess, A. Balducci, *J. Electrochem. Soc.* **2019**, *166*, A1763; c) J. Krummacher, C. Schütter, S. Passerini, A. Balducci, *ChemElectroChem* **2017**, *4*, 353–361; d) L. Köps, F. A. Kreth, D. Leistenschneider, K. Schutjajew, R. Gläßner, M. Oschatz, A. Balducci, *Adv. Energy Mater.* **2023**, *13*, 2203821; e) E. B. Pal, S. Yang, S. Ramesh, V. Thangadurai, R. Jose, *Nanoscale Advances* **2019**, *1*, 3807–3835; f) K. Xue, Z. Zheng, K. Su, X. Zhang, Y. Wang, J. Lang, *Chem. Eng. J.* **2024**, *491*, 152090; g) G. H. V. T. Nguyen, K. Kwak, K.-K. Lee, *Electrochim. Acta* **2019**, *299*, 98–106; h) H. X. Lu, J. M. Vicent-Luna, S. Calero, R. M. Madero-Castro, M. C. Gutiérrez, M. L. Ferrer, F. del Monte, *Energy Storage Mater.* **2021**, *40*, 368–385.
- [8] S. Pohlmann, C. Ramirez-Castro, A. Balducci, *J. Electrochem. Soc.* **2015**, *162*, A5020.
- [9] a) A. R. S. Kühnel, D. Reber, A. Remhof, R. Figi, D. Bleiner, C. Battaglia, *Chem. Commun.* **2016**, *52*, 10435–10438; b) B. J. Krummacher, L.-H. Heß, A. Balducci, *ChemSusChem* **2017**, *10*, 4178–4189; c) F. A. Kreth, L. Köps, C. Leibing, S. Darlami Magar, M. Hermesdorf, K. Schutjajew, C. Neumann, D. Leistenschneider, A. Turchanin, M. Oschatz, *Adv. Energy Mater.* **2024**, *24*, 2303909; d) D. P. Zaccagnini, L. H. Heß, L. Baudino, M. Laurenti, M. Serrapede, A. Lamberti, A. Balducci, *Adv. Mater. Interfaces* **2023**, *10*, 2202470; e) E. G. A. Elia, K. V. Kravchyk, M. V. Kovalenko, J. Chacón, A. Holland, R. G. A. Wills, *J. Power Sources* **2021**, *481*, 228870; f) F. S. Sayah, A. Ghosh, M. Baazizi, R. Amine, M. Dahbi, Y. Amine, F. Ghamouss, K. Amine, *Nano Energy* **2022**, *98*, 107336.
- [10] a) A. P. Meister, X. Qi, R. Kloepsch, E. Krämer, B. Streipert, M. Winter, T. Placke, *ChemSusChem* **2017**, *10*, 804–814; b) B. R.-S. Kühnel, M. Lübke, M. Winter, S. Passerini, A. Balducci, *J. Power Sources* **2012**, *214*, 178–184; c) C. R.-S. Kühnel, A. Balducci, *J. Power Sources* **2014**, *249*, 163–171.
- [11] R.-S. Kühnel, J. Reiter, S. Jeong, S. Passerini, A. Balducci, *Electrochem. Commun.* **2014**, *38*, 117–119.
- [12] a) A. K. Karuppasamy, P. A. Reddy, G. Srinivas, A. Tewari, R. Sharma, X. S. Shajan, D. Gupta, *J. Membr. Sci.* **2016**, *514*, 350–357; b) B. S. K. Hong, Y. Park, D. M. Pore, *Korean J. Chem. Eng.* **2014**, *31*, 1656–1660; c) C. A. Manivel, D. Velayutham, M. Noel, *J. Electroanal. Chem.* **2011**, *655*, 79–86; d) D. S. A. Forsyth, K. J. Fraser, P. C. Howlett, D. R. MacFarlane, M. Forsyth, *Green Chem.* **2006**, *8*, 256–261.
- [13] Eaton, Application guidelines, <https://www.eaton.com/content/dam/eaton/products/electronic-components/resources/technical/eaton-supercapacitor-application-guidelines.pdf>.
- [14] F. A. Kreth, L. Köps, S. W. Donne, A. Balducci, *Batteries & Supercaps* **2024**, e202300581.
- [15] X. Wang, E. Yasukawa, S. Mori, *Electrochim. Acta* **2000**, *45*, 2677–2684.
- [16] L. H. Heß, A. Balducci, *ChemSusChem* **2018**, *11*, 1919–1926.
- [17] L. H. Hess, L. Wittscher, A. Balducci, *Phys. Chem. Chem. Phys.* **2019**, *21*, 9089–9097.
- [18] L. Köps, F. A. Kreth, M. Klein, A. Balducci, *J. Power Sources* **2023**, *581*, 233480.
- [19] P. Ruschhaupt, S. Pohlmann, A. Varzi, S. Passerini, *Batteries & Supercaps* **2020**, *3*, 698–707.
- [20] J. W. Gittins, Y. Chen, S. Arnold, V. Augustyn, A. Balducci, T. Brousse, E. Frackowiak, P. Gómez-Romero, A. Kanwade, L. Köps, P. K. Jha, D. Lyu, M. Meo, D. Pandey, L. Pang, V. Presser, M. Rapisarda, D. Rueda-García, S. Saeed, P. M. Shirage, A. Ślesiński, F. Soavi, J. Thomas, M.-M. Titirici, H. Wang, Z. Xu, A. Yu, M. Zhang, A. C. Forse, *J. Power Sources* **2023**, *585*, 233637.
- [21] L. Köps, P. Zaccagnini, C. F. Pirri, A. Balducci, *Journal of Power Sources Advances* **2022**, *16*, 100098.

Manuscript received: April 25, 2024

Revised manuscript received: May 22, 2024

Accepted manuscript online: May 24, 2024

Version of record online: July 8, 2024